



# Statistical Survey of Coronal Mass Ejections and Interplanetary Type II Bursts

V. Krupar<sup>1,2,3</sup> , J. Magdalenic<sup>4</sup> , J. P. Eastwood<sup>5</sup> , N. Gopalswamy<sup>2</sup> , O. Kruparova<sup>3</sup> , A. Szabo<sup>2</sup> , and F. Němec<sup>6</sup> <sup>1</sup>Universities Space Research Association, Columbia, MD, USA; [vratislav.krupar@nasa.gov](mailto:vratislav.krupar@nasa.gov)<sup>2</sup>NASA Goddard Space Flight Center, Greenbelt, MD, USA; [nat.gopalswamy@nasa.gov](mailto:nat.gopalswamy@nasa.gov), [adam.szabo@nasa.gov](mailto:adam.szabo@nasa.gov)<sup>3</sup>Department of Space Physics, Institute of Atmospheric Physics, The Czech Academy of Sciences, Prague, Czech Republic; [ok@ufa.cas.cz](mailto:ok@ufa.cas.cz)<sup>4</sup>Solar-Terrestrial Center of Excellence-SIDC, Royal Observatory of Belgium, Brussels, Belgium; [jasmina.magdalenic@oma.be](mailto:jasmina.magdalenic@oma.be)<sup>5</sup>The Blackett Laboratory, Imperial College London, London, UK; [jonathan.eastwood@imperial.ac.uk](mailto:jonathan.eastwood@imperial.ac.uk)<sup>6</sup>Faculty of Mathematics and Physics, Charles University, Prague, Czech Republic; [frantisek.nemec@mff.cuni.cz](mailto:frantisek.nemec@mff.cuni.cz)

Received 2018 December 6; revised 2019 June 28; accepted 2019 July 16; published 2019 September 5

## Abstract

Coronal mass ejections (CMEs) are responsible for most severe space weather events, such as solar energetic particle events and geomagnetic storms at Earth. Type II radio bursts are slow drifting emissions produced by beams of suprathermal electrons accelerated at CME-driven shock waves propagating through the corona and interplanetary medium. Here, we report a statistical study of 153 interplanetary type II radio bursts observed by the two *STEREO* spacecraft between 2008 March and 2014 August. The shock associated radio emission was compared with CME parameters included in the Heliospheric Cataloguing, Analysis and Techniques Service catalog. We found that faster CMEs are statistically more likely to be associated with the interplanetary type II radio bursts. We correlate frequency drifts of interplanetary type II bursts with white-light observations to localize radio sources with respect to CMEs. Our results suggest that interplanetary type II bursts are more likely to have a source region situated closer to CME flanks than CME leading edge regions.

**Key words:** solar–terrestrial relations – Sun: coronal mass ejections (CMEs) – Sun: radio radiation

## 1. Introduction

Coronal mass ejections (CMEs) are large-scale magnetized plasma disturbances propagating through the corona and the interplanetary medium (Burlaga et al. 1987). CMEs are the most significant drivers of geomagnetic storms and thus of adverse space weather conditions. Type II bursts are generally considered to be associated with CME-driven shocks (Hansen et al. 1971; Gopalswamy 2011). They are generated, via a plasma emission mechanism, namely when electron beams accelerated at the shock fronts ahead of propagating CMEs interact with the ambient plasma producing radio emissions at the local plasma frequency  $f_p$  (the fundamental emission) and/or its second harmonic  $2f_p$  (the harmonic emission). As shocks propagate outward from the Sun, radio emission is generated at progressively lower frequencies corresponding to a decreasing ambient density (Ginzburg & Zhelezniakov 1958; Melrose 1980). Although type II bursts generated in the solar corona are frequently detected from the ground, spacecraft measurements show that type II bursts originating in the interplanetary medium occur more sporadically (Gopalswamy et al. 2001b, 2005; Vourlidis 2004; Miteva et al. 2017). Moreover, interplanetary type II bursts are usually patchy and intermittent with short periods of radio enhancements, which can be related to CME–CME and/or CME–streamer interactions (Gopalswamy et al. 2001a; Martínez Oliveros et al. 2012; Xie et al. 2012; Magdalenic et al. 2014; Krupar et al. 2016). Gopalswamy et al. (2005) analyzed a large number of type II bursts measured by the *Wind* spacecraft in conjunction with white-light observations of CMEs by the *Solar Heliospheric Observatory* (*SOHO*). They found that CMEs associated with

interplanetary type II bursts are typically more energetic and accompanied with more energetic flares than those associated with coronal type II bursts only. Gopalswamy et al. (2008) employed *SOHO* and *Wind* observations and found that faster CMEs are more likely to be associated with interplanetary type II bursts.

Here, we analyze white-light and radio measurements obtained by the twin-spacecraft *Solar Terrestrial Relations Observatory* (*STEREO*) mission (Kaiser et al. 2008). Both satellites were launched in 2006 October into heliocentric ecliptic orbits: *STEREO-A* moves ahead of the Earth in its orbit, while *STEREO-B* trails behind. We use data recorded by the Heliospheric Imager (HI; Howard et al. 2008; Eyles et al. 2009). The *STEREO*/HI instrument provides white-light images with coverage over solar elongation angles from  $4^\circ$  to nearly  $90^\circ$ , which allows us to track CMEs from  $\sim 8$  solar radii ( $1 R_\odot = 695,500$  km) up to Earth’s orbit at 1 astronomical unit ( $1 \text{ au} = 149,598,000$  km) and beyond.

The *STEREO*/WAVES instrument is dedicated to the investigation of solar radio emissions (Bale et al. 2008; Bougeret et al. 2008). We use data acquired by the *STEREO*/WAVES/High Frequency Receiver 1 (HFR1; 125 kHz–2 MHz), which allow us to analyze radio emissions located at distances from  $\sim 5 R_\odot$  above the Sun’s surface up to 0.4 au (Ceconi et al. 2008; Krupar et al. 2012, 2014). The Heliospheric Cataloguing, Analysis and Techniques Service (HELCASTS) project provides us with a catalog of both transient and background structures in the solar wind identified in the *STEREO*/HI data (Möstl et al. 2017; Harrison et al. 2018; Murray et al. 2018). Our analysis exploits CMEs included in the HELCASTS/HIGeoCAT catalog, which can be directly compared to radio measurements recorded by the *STEREO*/WAVES/HFR1 instrument due to an overlapping coverage of radial distances from the Sun. For the first time, we compare statistical properties of interplanetary type II bursts with CMEs observed by heliospheric imagers. In contrast,



Original content from this work may be used under the terms of the [Creative Commons Attribution 3.0 licence](https://creativecommons.org/licenses/by/3.0/). Any further distribution of this work must maintain attribution to the author(s) and the title of the work, journal citation and DOI.

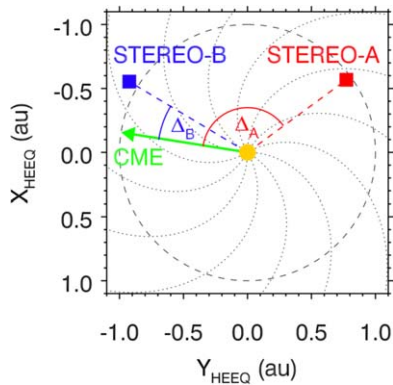


**Figure 1.** Positions of the spacecraft in the solar equatorial plane on 2012 October 22. The green arrow indicates the CME propagation direction obtained by the HMF technique.

previous studies exploited coronagraph measurements to retrieve CME parameters (e.g., Gopalswamy et al. 2008).

In this paper, we investigate the statistical properties of interplanetary type II radio bursts detected by *STEREO*/WAVES, and their relation with CMEs observed by *STEREO*/HI. In Section 2, we show an example of radio and white-light observations to demonstrate our analysis. In Section 3, we present statistical results on occurrence rates and relative radio source locations. Finally, the summary and conclusions are given in Section 4.

## 2. Observation and Analysis

Our statistical analysis is based on a list of interplanetary type II radio bursts detected by *STEREO*/WAVES and associated with CMEs observed by *STEREO*/HI included in the HELCATS/HIGeoCAT catalog ([https://www.helcats-fp7.eu/catalogues/wp3\\_cat.html](https://www.helcats-fp7.eu/catalogues/wp3_cat.html)). As an example from our list, we show the analysis of a type II radio burst from 2012 October 22. At the time of the event, the *STEREO-A* and *STEREO-B* spacecraft were  $126^\circ$  of heliocentric Earth equatorial (HEEQ) longitude ahead of and  $121^\circ$  behind the Earth, at heliocentric distances of 0.97 au and 1.08 au, respectively (Figure 1). *STEREO-B* detected the interplanetary type II radio bursts between 01:15 UT at 1.5 MHz and 10:30 UT at 125 kHz (Figure 2). The frequency drift was about  $41.29 \text{ Hz s}^{-1}$ . In this case, the radio emission was not observed by *STEREO-A*. We note that this type II burst was also observed by *Wind*/WAVES (<https://cdaw.gsfc.nasa.gov/>, Gopalswamy et al. 2009).

This interplanetary type II burst has been associated with a CME observed by the *STEREO-B*/HI instrument included in the HELCATS/HIGeoCAT catalog ([https://www.helcats-fp7.eu/catalogues/event\\_page.html?id=HCME\\_B\\_20121022\\_01](https://www.helcats-fp7.eu/catalogues/event_page.html?id=HCME_B_20121022_01)). Figure 2(c) shows a time-elongation profile (Jmap) between 2012 October 22 and 26 at the position angle of  $275^\circ$ . The CME propagation is denoted by red circles between 2012 October 22 04:54 UT at  $4^\circ.2$  elongation and 2012 October 25 19:18 UT at  $72^\circ.9$  elongation. The harmonic-mean fitting (HMF) technique is used to perform the elongation-to-distance conversion (Lugaz 2010). HMF assumes that a CME in the field of view (FOV) of *STEREO-B*/HI (i.e., in the interplanetary medium) propagates with a constant velocity and direction, and it has a circular shape anchored to the Sun at all times (Figure 3). We note that effects of observing CMEs at large angles must be taken into account because the assumption that CME brightness originates from the plane of sky is not

valid for the *STEREO*/HI FOV contrary to a typical coronagraph FOV (Möstl et al. 2011). HMF provides us with a CME speed of  $437 \pm 1 \text{ km s}^{-1}$ , a CME direction of  $99^\circ$  HEEQ longitude behind Earth, and a CME liftoff time of 17:49 UT on 2012 October 21. The CME was in the *STEREO-B*/HI FOV from 0.12 au up to 1.06 au, and the first three data points coincide with the radio emission interval (denoted by a green bar in Figure 2(c)). The angles between the CME direction and spacecraft locations are  $\Delta_A = 135^\circ$  and  $\Delta_B = 22^\circ$  for *STEREO-A* and *STEREO-B*, respectively (Figure 1). We note that this CME was also observed by coronagraphs on board *SOHO* and *STEREO-A* with a CME liftoff time of around 20:57 UT on 2012 October 21. The CME speed reached  $\sim 554 \text{ km s}^{-1}$  by the time it left the coronagraph FOV. A comparison between coronagraph and HI observations indicates that the CME possibly decelerated in the outer corona and/or the interplanetary medium. However, the large discrepancy in the liftoff times ( $\sim 3 \text{ hr}$ ) can also be attributed to different parts of the CME observed by the coronagraph and HI instruments. Nevertheless, we use the HI white-light data in this study hereafter.

We use the radial density gradient in the solar wind to investigate the relative locations of radio sources (Alvarez & Haddock 1973):

$$\frac{dn}{dr} = \frac{dn}{df} \frac{df}{dt} \frac{dt}{dr}, \quad (1)$$

where  $n$  is electron density,  $f$  is frequency,  $t$  is time, and  $r$  is radial distance. Next, we use the plasma frequency equation to obtain the following:

$$\frac{dn}{dr} = -\frac{2nD_f}{vf}, \quad (2)$$

where  $D_f$  is the frequency drift ( $D_f = \frac{f_1 - f_2}{t_2 - t_1} = -\frac{df}{dt}$ ), and  $v$  represents radial speed. We assume that below 2 MHz the shock is generally far enough that an  $n \sim r^{-2}$  dependence is valid (Gopalswamy 2011). Then we may write the following:

$$r = \frac{vf}{D_f}. \quad (3)$$

Finally, we assume that the radio source speed  $v$  is equal to the white-light speed  $v_{\text{WL}}$  of a CME retrieved by the HMF technique, which assumes a spherical shape for CMEs attached to the Sun. We may compare the deviation  $r_{\text{WL}}$  from radio source height  $r$  (Figure 3):

$$\xi = \cos^{-1}\left(\frac{r}{r_{\text{WL}}}\right) = \cos^{-1}\left(\frac{fv_{\text{WL}}}{D_f r_{\text{WL}}}\right). \quad (4)$$

Specifically, we correlate the frequency drift with the CME speed and location retrieved from the white-light measurements. Using this method, we are able to estimate the relative radio source locations to the CME propagation direction. From radio and white-light observations ( $f = 812.5 \text{ kHz}$ ,  $v_{\text{WL}} = 437 \text{ km s}^{-1}$ ,  $D_f = 41.29 \text{ Hz s}^{-1}$ , and  $r_{\text{WL}} = 27.72 R_S$ ), we calculate  $\xi$  to be  $63^\circ.5$  for this radio emission. It corresponds to a scenario of a type II radio burst arising from the CME flank.

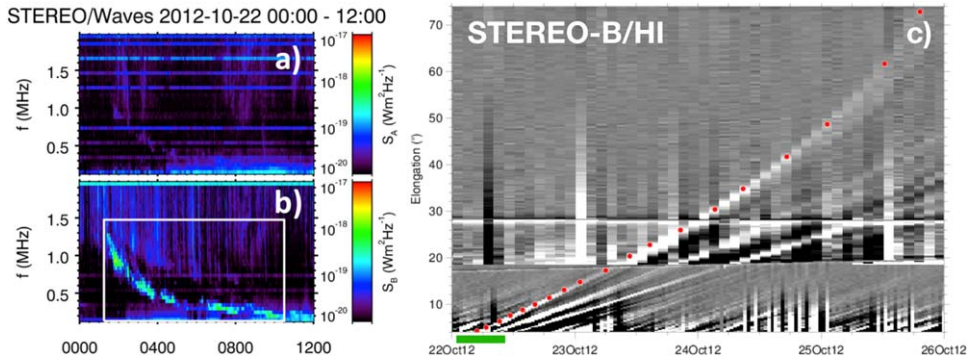


**Figure 2.** Radio and white-light measurements by *STEREO*. (a), (b) Radio flux density  $S$  between 2012 October 22 00:00 UT and 12:00 UT at *STEREO-A* and *STEREO-B*, respectively. A white rectangle denotes the type II burst. (c) *STEREO-B/HI* time-elongation map between 2012 October 22 and 26 (adapted from [https://www.helcats-fp7.eu/catalogues/event\\_page.html?id=HCME\\_B\\_20121022\\_01](https://www.helcats-fp7.eu/catalogues/event_page.html?id=HCME_B_20121022_01)). Positions of the CME are denoted as red circles. A green bar shows a time interval with the radio emission.

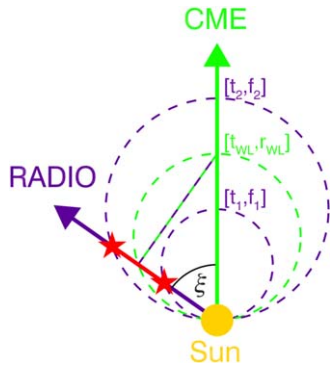


**Figure 3.** Schematic illustration showing an interpretation of the propagation angle  $\xi$  of CMEs and associated radio emissions. The red line segment and stars indicate estimated type II burst source locations.

### 3. Statistical Results

We have compared *STEREO/WAVES* measurements of type II radio bursts with CMEs included in the HELCATS/HIGeoCAT catalog between 2007 and 2014. During this period, 1351 CMEs were manually identified in the *STEREO/HI* data (Harrison et al. 2018). Figure 4(a) shows the distribution of these CMEs versus time. As expected, CMEs were predominantly observed during the high level of solar activity near solar maximum (Figure 4(d), Gopalswamy et al. 2015). We have found 156 interplanetary type II radio bursts detected by *STEREO/WAVES* associated with *STEREO/HI* CMEs (Figure 4(b)). We have also found that 11% of *STEREO/HI* CMEs are associated with interplanetary type II radio bursts (Figure 4(c)). Two-sample Anderson–Darling rank test (Pettitt 1976) reveals that the temporal distributions of CMEs with and without radio emissions are different (statistical significance principally 100%). Furthermore, it turns out that the CMEs are more likely to be associated with the radio emissions during larger solar activity (Kendall’s tau coefficient of about 0.70, principally 100% statistically significant). We note that only one interplanetary type II radio burst occurred during the period of the solar minimum between 2007 and 2010.

Figures 5(a) and (b) show distributions of all CMEs and CMEs associated with radio emissions versus CME speed, respectively. The Two-sample Anderson–Darling test reveals that the speed distributions of CMEs with and without radio emissions are different (statistical significance principally

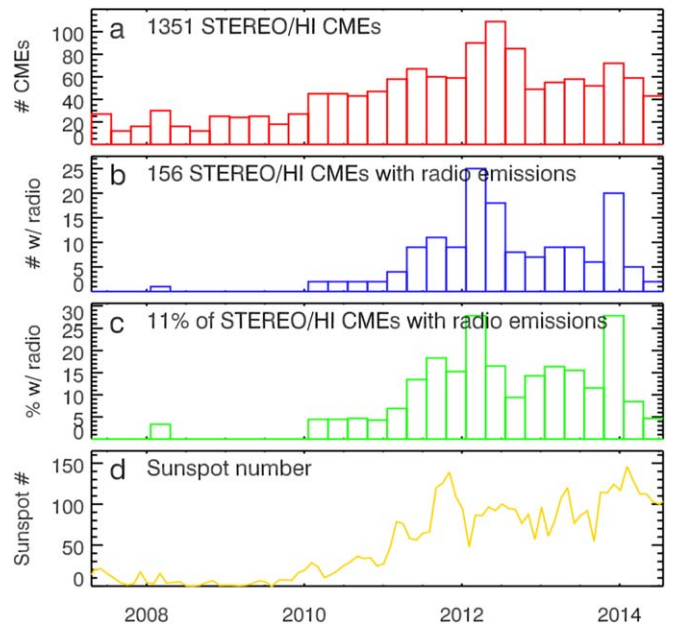


**Figure 4.** Statistical results. (a) Distribution of CMEs included in the HELCATS CME catalog, (b) number of CMEs associated with radio emissions, (c) percentage of CMEs associated with radio emissions, and (d) sunspot number vs. time.

100%). The average speed of CMEs with interplanetary type II bursts is  $945 \text{ km s}^{-1}$ , while that of all CMEs is  $639 \text{ km s}^{-1}$ . Our results thus indicate that faster CMEs are considerably more likely to be associated with interplanetary type II radio bursts when compared to slower CMEs (Figure 5(c), Kendall’s tau coefficient of about 0.59, principally 100% statistically significant). This result is consistent with previous studies that used coronagraph observations (e.g., Gopalswamy et al. 2008). Generally, faster CMEs are believed to be more energetic and thus likely to be associated with stronger shock waves, which produce interplanetary type II bursts (Gopalswamy et al. 2005).

Subsequently, we have investigated the visibility of CMEs with and without interplanetary type II bursts (Figure 6). We note that each *STEREO/HI* CME propagation direction is correlated with both *STEREO-A* and *STEREO-B* locations separately. Specifically, we have analyzed 2702  $\Delta$  angles in total. We have obtained almost uniform distributions of angles  $\Delta$  for all events included in the HELCATS/HIGeoCAT catalog (Figure 6(a)). However, those associated with radio

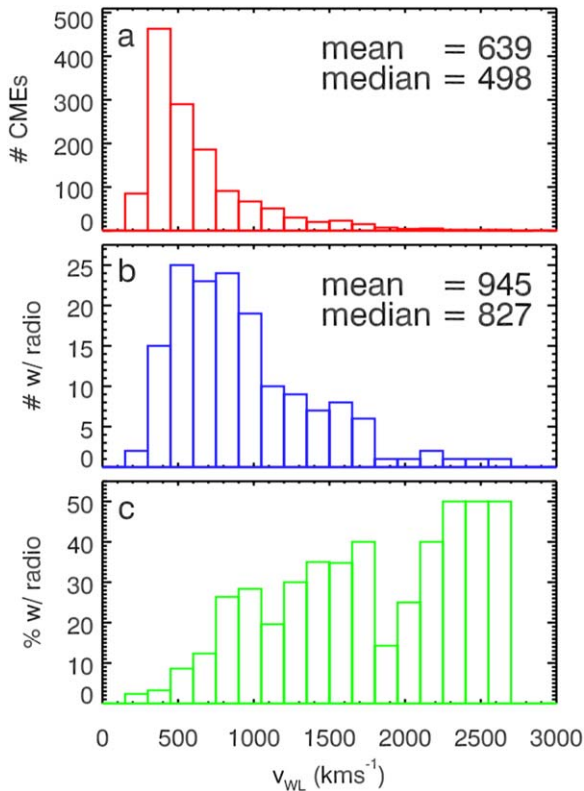


**Figure 5.** Statistical results. (a) Distribution of CMEs included in the HELCATS CME catalog, (b) number of CMEs associated with radio emissions, and (c) percentage of CMEs associated with radio emissions vs. CME speed.

emissions indicate a reduced visibility of *STEREO*/HI CMEs propagating toward the spacecraft by  $\sim 50\%$ , when compared to CMEs propagating perpendicular to the Sun-spacecraft direction (Figures 6(b) and (c)). Two-sample Anderson–Darling test indeed reveals that the distributions of the propagation directions of CMEs with and without radio emissions are different with a statistical significance of about 99.3%. The Kendall’s tau coefficient between the angle  $\Delta$  and the percentage of CMEs associated with radio emissions is about 0.44, and its statistical significance is about 95%. The reduced visibility can be related to a scenario where a CME forms an obstacle for radio emissions with source regions located closer to the CME flanks than to the CME leading edge regions.

Finally, we have statistically analyzed the deviations of radio source locations from CME directions  $\xi$  (Figure 7). We assume the presence of the fundamental emission unless we observe both components. The obtained distribution of  $\xi$  angles ranges from  $15^\circ$  to  $90^\circ$  with the average value of  $62.3^\circ$ . Our results suggest that the source region of interplanetary type II bursts appear predominantly close to the CME flanks instead of the CME leading edge. As a possible explanation of this result we note that CME–CME and/or CME–streamer interactions are more likely to occur closer to CME flanks than to CME leading edge regions.

#### 4. Summary and Conclusion

We present a statistical study of 153 interplanetary type II radio bursts observed by the two *STEREO* spacecraft between 2008 March and 2014 August. We analyzed the 2012 October

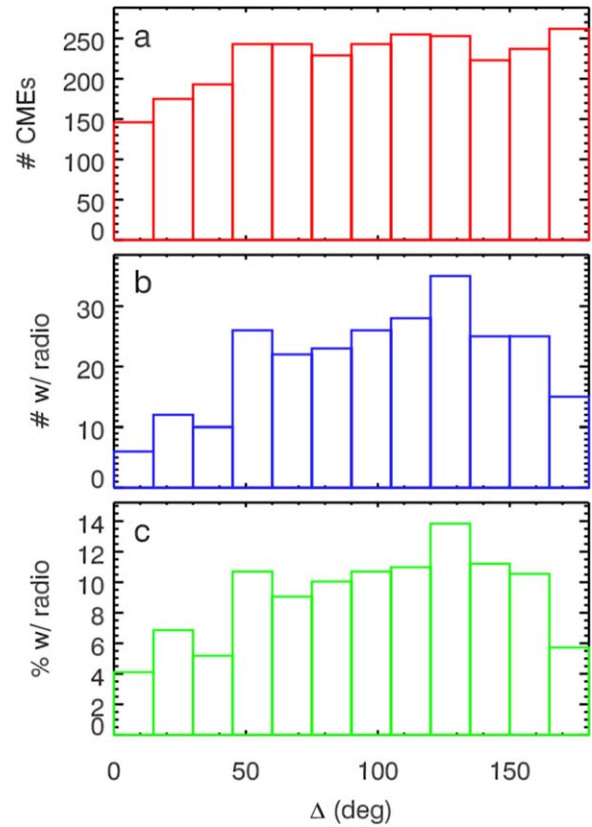


**Figure 6.** Statistical results. (a) Distribution of CMEs included in the HELCATS CME catalog, (b) number of CMEs associated with radio emissions, and (c) percentage of CMEs associated with radio emissions vs. angles between the CME direction and spacecraft location  $\Delta$ .

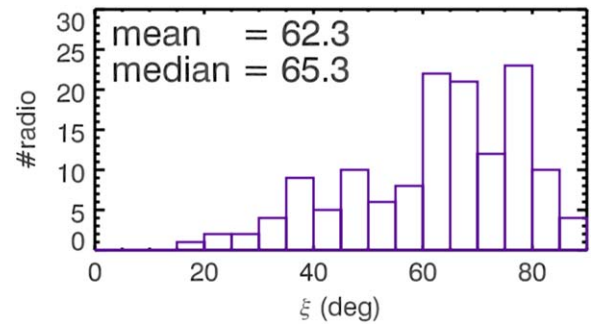


**Figure 7.** Statistical results. Histogram of deviations of radio source locations from CME directions  $\xi$ .

22 CME to demonstrate our technique (Figures 1 and 2). We showed how to estimate the deviation of radio sources from the CME propagation direction (Figure 3). The shock-associated radio emissions were compared with *STEREO*/HI CMEs from the HELCATS/HIGeoCAT catalog (Figure 4). Based on a statistical survey, in which we analyze large FOV *STEREO*/HI observations that were never employed in such a study before, we conclude that fast CMEs are statistically more likely to be associated with interplanetary type II radio bursts (Figure 5). This work therefore confirms a known relationship of shock formation and radio waves generation. We also studied the visibility of interplanetary type II radio bursts with respect to spacecraft locations (Figure 6). Our results indicate that *STEREO*/HI CMEs with associated radio emissions are less likely to be observed when they propagate toward the

spacecraft. We correlate frequency drifts of radio emission with white-light observations to localize radio sources with respect to the CME geometry (Figure 7). Our results suggest that interplanetary type II bursts are more likely to have a source region situated close to CME flanks instead of the CME nose. CMEs then form an obstacle for radio emissions due to increased plasma density and larger magnetic field, characteristic of CMEs. Only additional processes, such as CME–CME and/or CME–streamer interactions, may lead to amplification of the radio signal that can be consequently remotely detected by space-based instruments located at large distances. We suggest that a prospective space-borne radio instrumentation located at the fourth and/or fifth Sun–Earth Lagrangian points—due to the preferential generation site at CME flanks—would provide us with additional information about speeds and directions of fast and potentially geoeffective CMEs with possible space weather applications.

The authors would like to thank the many individuals and institutions who contributed to making *STEREO* possible. V.K. acknowledges support by an appointment to the NASA postdoctoral program at the NASA Goddard Space Flight Center administered by Universities Space Research Association under contract with NASA and the Czech Science Foundation grant 17-06818Y. O.K. acknowledges the support of the Czech Science Foundation grant 17-06065S. This work has been supported by the Praemium Academiae award by the Czech Academy of Sciences, and the European Union Seventh Framework Programme (FP7/2007–2013) under grant agreement No. 606692 (HELCASTS).

#### ORCID iDs

V. Krupar  <https://orcid.org/0000-0001-6185-3945>  
 J. Magdalenic  <https://orcid.org/0000-0003-1169-3722>  
 J. P. Eastwood  <https://orcid.org/0000-0003-4733-8319>  
 N. Gopalswamy  <https://orcid.org/0000-0001-5894-9954>  
 O. Kruparova  <https://orcid.org/0000-0002-1122-6422>  
 A. Szabo  <https://orcid.org/0000-0003-3255-9071>

F. Němec  <https://orcid.org/F.Nemec.0000-0002-3233-2718>

#### References

- Alvarez, H., & Haddock, F. T. 1973, *SoPh*, **29**, 197  
 Bale, S. D., Ullrich, R., Goetz, K., et al. 2008, *SSRv*, **136**, 529  
 Bougeret, J. L., Goetz, K., Kaiser, M.L., et al. 2008, *SSRv*, **136**, 487  
 Burlaga, L. F., Behannon, K. W., & Klein, L. W. 1987, *JGR*, **92**, 5725  
 Cecconi, B., Bonnin, X., Hoang, S., et al. 2008, *SSRv*, **136**, 549  
 Eyles, C. J., Harrison, R.A., Davis, C.J., et al. 2009, *SoPh*, **254**, 387  
 Ginzburg, V. L., & Zhelezniakov, V. V. 1958, *SvA*, **2**, 653  
 Gopalswamy, N. 2011, Planetary Radio Emissions VII, ed. H.O. Rucker, (Vienna: Austrian Academy of Sciences Press), 325  
 Gopalswamy, N., Aguilar-Rodriguez, E., Yashiro, S., et al. 2005, *JGRA*, **110**, A12S07  
 Gopalswamy, N., Makela, P., Akiyama, S., Yashiro, S., & Thakur, N. 2015, *SunGe*, **10**, 111  
 Gopalswamy, N., Yashiro, S., Akiyama, S., et al. 2008, *AnGeo*, **26**, 3033  
 Gopalswamy, N., Yashiro, S., Kaiser, M. L., Howard, R. A., & Bougeret, J.-L. 2001a, *ApJL*, **548**, L91  
 Gopalswamy, N., Yashiro, S., Kaiser, M. L., Howard, R. A., & Bougeret, J.-L. 2001b, *JGR*, **106**, 29219  
 Gopalswamy, N., Yashiro, S., Michalek, G., et al. 2009, *EM&P*, **104**, 295  
 Hansen, R. T., Garcia, C. J., Grogard, R. J.-M., & Sheridan, K. V. 1971, *PASau*, **2**, 57  
 Harrison, R. A., Davies, J., Barnes, D., et al. 2018, *SoPh*, **293**, 77  
 Howard, R. A., Moses, J.D., Vourlidas, A., et al. 2008, *SSRv*, **136**, 67  
 Kaiser, M. L., Kucera, T. A., Davila, J. M., et al. 2008, *SSRv*, **136**, 5  
 Krupar, V., Maksimovic, M., Santolik, O., Cecconi, B., & Kruparova, O. 2014, *SoPh*, **289**, 4633  
 Krupar, V., Santolik, O., Cecconi, B., et al. 2012, *JGRA*, **117**, A06101  
 Krupar, V., Eastwood, J.P., Kruparova, O., et al. 2016, *ApJL*, **823**, L5  
 Lugaz, N. 2010, *SoPh*, **267**, 411  
 Magdalenic, J., Marqué, C., Krupar, V., et al. 2014, *ApJ*, **791**, 115  
 Martínez Oliveros, J. C., Lindsey, C., Bale, S. D., & Krucker, S. 2012, *SoPh*, **279**, 153  
 Melrose, D. B. 1980, *SSRv*, **26**, 3  
 Miteva, R., Samwel, S. W., & Krupar, V. 2017, *JSWSC*, **7**, A37  
 Möstl, C., Rollett, T., Lugaz, N., et al. 2011, *ApJ*, **741**, 34  
 Möstl, C., Isavnin, A., Boakes, P.D., et al. 2017, *SpWea*, **15**, 955  
 Murray, S. A., Guerra, J. A., Zucca, P., et al. 2018, *SoPh*, **293**, 60  
 Pettitt, A. N. 1976, *Biometrika*, **63**, 161  
 Vourlidas, A. 2004, *ASSL*, **314**, 223  
 Xie, H., Odstreil, D., Mays, L., et al. 2012, *JGRA*, **117**, A04105